Impact of general reionization scenarios on extraction of inflationary parameters

Stefania Pandolfi,[1,2] Elena Giusarma,[3] Edward W. Kolb,[4] Massimiliano Lattanzi[1],
Alessandro Melchiorri[2], Olga Mena[3], Manuel Peña[3], Asantha Cooray,[5] and Paolo Serra[5]

[1] *Physics Department and ICRA, Universita' di Roma "La Sapienza", Ple. Aldo Moro 2, 00185, Rome, Italy*
[2] *Physics Department and INFN, Universita' di Roma "La Sapienza", Ple. Aldo Moro 2, 00185, Rome, Italy*
[3] *IFIC, Universidad de Valencia-CSIC, 46071, Valencia, Spain*
[4] *Department of Astronomy & Astrophysics, Enrico Fermi Institute, and Kavli Institute for Cosmological Physics, University of Chicago, Chicago, Illinois 60637, USA*
[5] *Center for Cosmology, Department of Physics & Astronomy, University of California, Irvine, California 92697, USA*

Determination of whether the Harrison–Zel'dovich spectrum for primordial scalar perturbations is consistent with observations is sensitive to assumptions about the reionization scenario. In light of this result, we revisit constraints on inflationary models using more general reionization scenarios. While the bounds on the tensor-to-scalar ratio are largely unmodified, when different reionization schemes are addressed, hybrid models are back into the inflationary game. In the general reionization picture, we reconstruct both the shape and amplitude of the inflaton potential. We find a broader spectrum of potential shapes when relaxing the simple reionization restriction. An upper limit of 10^{16} GeV to the amplitude of the potential is found, regardless of the assumptions on the reionization history.

PACS numbers: 98.80.-k 95.85.Sz, 98.70.Vc, 98.80.Cq

I. INTRODUCTION

The inflationary paradigm seems to be the ideal mechanism not only for solving cosmological paradoxes such as the observed large-scale smoothness and spatial flatness of our universe, but also for providing the initial seeds for structure formation. The simplest inflationary model makes use of a single scalar field ϕ (the inflaton), which slowly evolves in a very shallow, nearly constant, potential $V(\phi)$. The dynamics of slow roll gives rise to a quasi-de Sitter phase of exponential expansion in the very early universe. Since the slope of the spectrum is closely related to derivatives of the field potential, slow-roll dynamics predicts that the perturbation spectra should be very close to scale invariant, although not *exactly* so. This implies that a quite general inflationary prediction is that the power spectra of both scalar, $P_{\mathcal{R}}$, and tensor, P_T, fluctuations can be well approximated by power laws, *i.e.,*

$$P_{\mathcal{R}}(k) \propto k^{n-1}, \quad P_T(k) \propto k^{n_T}, \tag{1}$$

where the spectral indices n and n_T have very mild, if any, dependence on the scale k. A scale-invariant scalar power spectrum corresponding to the value $n = 1$ is the model proposed by Harrison, Zel'dovich, and Peebles [1]. In other words, from all the considerations above, inflation predicts $n \simeq 1$, but usually $n \neq 1$.[1]

A value of the spectral index n slightly different from unity would strongly point to the inflationary paradigm as the mechanism responsible for providing the initial conditions for structure formation. In addition, in many inflationary models the amplitude of gravitational waves is proportional to $|n - 1|$. Confirmation of a deviation from a scale-invariant power spectrum would encourage the gravitational waves hunters to keep searching for the detection of a nonzero tensor amplitude.

The most recent analysis by the Wilkinson Microwave Anisotropy Probe (WMAP) team of their seven-year data [3] rule out the Harrison-Zel'dovich (H–Z) primordial power spectrum at more than 3σ when ignoring tensor modes: $n = 0.963 \pm 0.012$. But this, as well as most other previously derived constraints from CMB data on cosmological parameters have assumed a "sudden" and complete reionization at a single redshift z_r. The reionization redshift, z_r, is taken to be in the range $4 < z_r < 32$, and the cosmological constraints are obtained after marginalization over z_r. The electron ionization fraction $x_e(z)$ is such that for $z \ll z_r$ $x_e(z) = 1$ ($x_e(z) = 1.08$ for $z < 3$ in order to take into account Helium recombination) and $x_e(z) = 2\times10^{-4}$ for $z > z_r$, *i.e.,* joining the value after primordial recombination with a smooth interpolation.

The process of structure formation that led to gravitational collapse of objects in which the first stars formed are still subject to theoretical and observational uncertainties. As these first sources began to illuminate their local neighborhoods, the HI present in the IGM was "reionized." The end of the Dark Ages (the period between the end of CMB recombination and the appearance of the first stars) remains to be explored and understood.

There are two main effects on the CMB anisotropies produced by the free electrons of the ionized gas: the first one washes out the primary anisotropies of the temperature autocorrelation (TT) spectrum. The damping of the TT signal is quantified by the optical depth parameter

[1] For a discussion of slow-roll inflation models with $n = 1$, see Ref. [2].

τ, proportional to the column density of ionized hydrogen. Earlier reionization leads to a the larger suppression of the TT acoustic peaks. The second effect produces a damping and an additional peak in the polarization autocorrelation spectrum (EE) [4]. The position of this new peak in the polarization signal is proportional to the square root of the redshift at which the reionization occurs, and its amplitude is proportional to the optical depth. Since the precise details of reionization processes are currently unknown, it is mandatory to explore the imprints of general reionization histories on the CMB spectra. In the standard, sudden reionization scenario, the EE spectrum depends exclusively on the value of Thomson optical depth τ. In turn, in extended reionization schemes, the precise history of how the universe became ionized affects the large-scale EE power spectrum in a crucial way [5], and the power is transferred from larger to smaller scales when considering that reionization processes could take place in a non-negligible redshift (time) interval.

The major goal of this paper is to study how current constraints on the scalar spectral index n and the tensor-to-scalar ratio r are modified if the standard ("sudden") reionization assumption is relaxed. In a precursor study we demonstrated that in a general reionization scenario the Harrison-Zel'dovich spectrum ($n = 1$) is perfectly consistent with observations [6]. In this study we shall also include information from tensors modes, showing that inflationary models that are ruled out in the sudden reionization scheme are allowed in more general reionization scenarios. We also reconstruct both the shape and the amplitude of the inflationary potential $V(\phi)$ allowed by current data in both sudden and general reionization schemes.

The paper is organized as follows. Section II summarizes the results of inflationary theory relevant for our considerations. A possible classification of different models of inflation is presented in Sec. III. The analysis method used here to derive the cosmological constraints is described in Sec. IV. Section V gives the resulting constraints on cosmological parameters and their implications for inflationary models. The inflationary potential reconstruction method and the results are presented in Sec. VI. We conclude in Sec. VII.

II. INFLATION AND THE HAMILTON-JACOBI FORMALISM

In this section we briefly review the dynamics of a scalar field in a cosmological background. We assume a flat Friedmann-Robertson-Walker (FRW) metric:

$$ds^2 = dt^2 - a^2(t)[dr^2 + r^2 d\Omega^2] \ , \tag{2}$$

where $a(t)$ is the cosmological scale factor. In an FRW background, a scalar field ϕ evolves under the action of potential $V(\phi)$ with equations of motion

$$\ddot{\phi} + 3H\dot{\phi} + V'(\phi) = 0 \ , \tag{3}$$

$$H^2 = \frac{8\pi}{3m_{\rm Pl}^2}\left[\frac{1}{2}\dot{\phi}^2 + V(\phi)\right] \ , \tag{4}$$

where $H \equiv \dot{a}/a$ is the Hubble parameter, dots and primes denote derivatives with respect to cosmological time and to the scalar field respectively, and $m_{\rm Pl}$ is the Planck mass. From the definition of the Hubble parameter, it follows that

$$a(t) \propto e^{-N} = \exp\left[\int_{t_o}^{t} H(t)dt\right] \ , \tag{5}$$

where the number of e-folds N is simply

$$N \equiv \int_{t}^{t_e} H(t)dt \ , \tag{6}$$

where t_e refers to the end on inflation. The integration extrema are chosen in such a way that $N = 0$ coincides with the end of inflation.

A very powerful way of describing the inflationary dynamics is given by the Hamilton-Jacobi formulation of inflation. The basic idea is to consider the scalar field ϕ itself to be the time variable; this can be done as long as it varies monotonically with time. Then, expressing the Hubble parameter as a function of the field, $H = H(\phi)$, the equations of motion become

$$\dot{\phi} = -\frac{m_{\rm Pl}^2}{4\pi}H'(\phi), \tag{7}$$

$$[H'(\phi)]^2 - \frac{12\pi}{m_{\rm Pl}^2}H^2(\phi) = -\frac{32\pi^2}{m_{\rm Pl}^4}V(\phi). \tag{8}$$

The second of these equations is called the Hamilton-Jacobi equation. Inflation takes place while the field is slowly rolling towards a minimum of the potential, and the field energy density is dominated by its potential energy. More quantitatively, the slow-roll approximation holds in the limit in which $\ddot{\phi} \ll 3H\dot{\phi}$ and $\dot{\phi}^2 \ll V$, so that Eqs. (3) and (4) become

$$\dot{\phi} \simeq -\frac{V'(\phi)}{3H} \ ,$$

$$H^2 \simeq \frac{8\pi}{3m_{\rm Pl}^2}V(\phi) \ . \tag{9}$$

The validity of the slow-roll approximation is quite natural because the slope of the inflaton potential must be sufficiently shallow to drive inflation. For single-field inflation during the slow-roll phase, the kinetic energy of the field is negligible and the potential is nearly constant:

$$\rho_\phi = V(\phi) + \frac{\dot{\phi}^2}{2} \simeq V(\phi) \simeq \text{const.} \tag{10}$$

From Eq. (9), we can see that this gives rise to a (quasi-) de Sitter phase with H almost constant. The amplitude

of the potential must be sufficiently large to dominate the energy density of the Universe at that epoch.

The slow-roll approximation is consistent if both the slope and the curvature of the potential are small (in units of the Planck mass) when compared to the potential itself: $V', V'' \ll V$, or equivalently if the so-called slow-roll parameters ϵ and η are much smaller than unity. The slow-roll parameters are defined as

$$\epsilon \equiv \frac{m_{\rm Pl}^2}{4\pi}\left[\frac{H'}{H}\right]^2 , \qquad \eta \equiv \frac{m_{\rm Pl}^2}{4\pi}\left[\frac{H''}{H}\right] . \tag{11}$$

When $V', V'' \ll V$, both ϵ and η can be expressed in terms of the potential and its derivatives as

$$\epsilon \simeq \frac{m_{\rm Pl}^2}{16\pi}\left(\frac{V'}{V}\right)^2 \ll 1 \ ,$$
$$\eta \simeq \frac{m_{\rm Pl}^2}{8\pi}\left[\frac{V''}{V} - \frac{1}{2}\left(\frac{V'}{V}\right)^2\right] \ll 1 \ . \tag{12}$$

The consistency of the slow-roll condition thus implies that $\epsilon, |\eta| \ll 1$. Using the definition of ϵ, the Hamilton-Jacobi equation can be rewritten in the useful form

$$H^2(\phi)\left[1 - \frac{1}{3}\epsilon(\phi)\right] = \frac{8\pi}{3m_{\rm Pl}^2}V(\phi) \ . \tag{13}$$

Inflation also provides a natural mechanism to generate the inhomogeneities presently observed in the Universe. During inflation, quantum fluctuations, inevitably present at small scales, are quickly redshifted to scales much larger than the horizon size and then frozen in as perturbations to the background metric. The perturbations created during inflation can be of two types: scalar (or curvature) perturbations, which couple to the matter stress-energy tensor, and tensor perturbations (gravitational waves), which do not couple to matter. The power spectrum of scalar perturbations (quantified as perturbations in the Ricci scalar $\mathcal{R}$) is described by

$$P_{\mathcal{R}}^{1/2}(k) = \left(\frac{H^2}{2\pi|\dot{\phi}|}\right)_{k=aH} = \left[\frac{H}{\sqrt{\pi}m_{\rm Pl}}\frac{1}{\sqrt{\epsilon}}\right] , \tag{14}$$

and its spectral index n reads

$$n - 1 \equiv \frac{d\ln P_{\mathcal{R}}}{d\ln k} \ . \tag{15}$$

The power spectrum of tensor fluctuation modes is given by

$$P_T^{1/2}(k) = \left(\frac{4}{\sqrt{\pi}}\frac{H}{m_{\rm Pl}}\right)_{k=aH} , \tag{16}$$

again evaluated when the mode k crosses the horizon.

The ratio of the tensor-to-scalar perturbation is defined as

$$\frac{P_T}{P_{\mathcal{R}}} \equiv r \ , \tag{17}$$

and, as in the scalar power spectrum case, one can write $P_T \propto k^{n_T}$. The two spectral indices expressed in terms of the slow-roll parameters are

$$n \simeq 1 - 4\epsilon + 2\eta \ , \tag{18}$$
$$n_T \simeq -2\epsilon \ , \tag{19}$$

and the tensor-to-scalar ratio r is

$$r \equiv 16\epsilon \ . \tag{20}$$

The relations above are valid at first-order approximation in the slow-roll parameters. Therefore, if primordial perturbations originated from the dynamics of a slow-rolling scalar field, the spectrum should not be exactly scale invariant. In fact, since the slow-roll parameters ϵ and η are small, but not vanishing (in other words, since the potential is very close to flat but not *exactly* flat), we expect that $n \simeq 1$ but nevertheless $n \neq 1$. A scale-invariant power spectrum corresponds to the value $n = 1$ is the aforementioned model proposed by Harrison, Zel'dovich, and Peebles [1]. Given the fact that $P_{\mathcal{R}} \propto k^{n-1}$, the spectral index can be thought as a measure of the departure of the spectrum of the scalar perturbations from an exactly scale-invariant power spectrum.

III. ZOOLOGY OF INFLATIONARY MODELS

In this section we follow the classification of Kinney *et al.* [7]. At lowest order in the slow-roll approximation the relevant parameters to distinguish among inflationary models are n and r [8]. The different classes of models are characterized by the relation between these two parameters, or equivalently, by the relation between ϵ and η. At lowest order in the slow-roll approximation we can divide the inflationary models into three general types: *large-field*, *small-field* and *hybrid*. The boundary between large-field and small-field models is represented by the so called *linear* models.

- Large-field models are characterized by $-\epsilon < \eta \leq \epsilon$. Popular examples of large-field models are $V(\phi) = \Lambda^4(\phi/\mu)^p$ and exponential potentials, $V(\phi) = \Lambda^4 \exp(\phi/\mu)$.

- Small-field models are characterized by $\eta < -\epsilon$. They result from a generic potential of the form $V(\phi) = \Lambda^4[1 - (\phi/\mu)^p]$, which can be understood as the lowest-order Taylor expansion of an arbitrary potential about the origin.

- Hybrid models are characterized by $0 < \epsilon < \eta$. A generic hybrid potential is of the form $V(\phi) = \Lambda^4[1 + (\phi/\mu)^p]$.

- Linear models are on the boundary between large-field and small-field, and they are characterized for this reason by $\eta = -\epsilon$. The generic linear potential is of the form: $V(\phi) \propto \phi$.

With the above classification we can cover the entire n-r plane and derive constraints on the inflationary models directly from the constraints on the n-r plane that arise from cosmological observations; see Sec. V.

IV. ANALYSIS METHOD

We adopt two different methods for parametrization of the reionization history. The first method, developed in Ref. [5], is based on principal components that provide a complete basis for describing the effects of reionization on large-scale E-mode polarization. Following Ref. [5], one can parametrize the reionization history as a free function of redshift by decomposing $x_e(z)$ into its principal components:

$$x_e(z) = x_e^f(z) + \sum_\mu m_\mu S_\mu(z), \tag{21}$$

where the principal components, $S_\mu(z)$, are the eigenfunctions of the Fisher matrix that describes the dependence of the polarization spectra on the electron ionization fraction $x_e(z)$, m_μ are the amplitudes of the principal components for a particular reionization history, and $x_e^f(z)$ is the WMAP fiducial model at which the Fisher matrix is computed and from which the principal components are obtained. In what follows we use the publicly available $S_\mu(z)$ functions and vary the amplitudes m_μ for $\mu = 1, ..., 5$ for the first five eigenfunctions. Hereafter we refer to this method as the MH (Mortonson-Hu) case.

In a second approach to a general reionization prescription we employ a different parametrization, sampling the evolution of the ionization fraction x_e as a function of redshift z at seven points ($z = 9, 12, 15, 18, 21, 24,$ and 27), and interpolating the value of $x_e(z)$ between them with a cubic spline. For $30 < z$ we fix $x_e = 2 \times 10^{-4}$ as the value of x_e expected before reionization (and after primordial recombination), while $x_e = 1$ for $3 < z < 6$ and $x_e = 1.08$ for $z < 3$ in order to be in agreement with both Helium ionization and Gunn-Peterson test observations. This approach is very similar to the one used in Ref. [9], and we will refer to it as the LWB (Lewis-Weller-Battye) case.

We then modified the Boltzmann CAMB code [10], incorporating the two generalized reionization scenarios and extracted cosmological parameters from current data using a Monte Carlo Markov Chain (MCMC) analysis based on the publicly available MCMC package `cosmomc` [11].

We consider here a flat ΛCDM universe described by a set of cosmological parameters

$$\{\omega_b, \omega_c, \Theta_s, n, \log[10^{10} A_s], r, n_{run}\}, \tag{22}$$

where $\omega_b \equiv \Omega_b h^2$ and $\omega_c \equiv \Omega_c h^2$ are the physical baryon and cold dark matter densities relative to the critical density, Θ_s is the ratio between the sound horizon and the angular diameter distance at decoupling, A_s is the amplitude of the primordial spectrum, n is the scalar spectral index, r is the tensor-to-scalar ratio, and $n_{run} \equiv dn/d\ln k$ is the running of the scalar spectral index:

$$\Delta^2_{\mathcal{R}}(k) = \Delta^2_{\mathcal{R}}(k_0) \left(\frac{k}{k_0}\right)^{n(k_0)-1+\frac{1}{2}\ln(k/k_0)dn/d\ln k}. \tag{23}$$

Here, $k_0 = 0.002$ Mpc^{-1} is the pivot scale.

The extra parameters needed to describe reionization are the five amplitudes of the eigenfunctions for the MH case, or the seven amplitudes in the seven bins for the LWB case, and one single common parameter, the optical depth, τ, for the sudden reionization case.

Our basic data set is the seven–year WMAP data [3] (temperature, polarization, and tensor modes) with the routine for computing the likelihood supplied by the WMAP team. Together with the WMAP data, we also augment the WMAP7 data with the CMB data sets from BOOMERanG [12], QUAD [13], ACBAR [14], and BICEP [15]. For all these experiments we marginalize over a possible contamination from the Sunyaev-Zel'dovich component, rescaling the WMAP template at the corresponding experimental frequencies. We therefore consider two cases: we first analyze the WMAP data alone, referring to it as to the "WMAP7" case, and we then include the remaining CMB experiments ("CMB-ALL").

V. RESULTS

Table I summarizes the main results of the analysis for different cosmological data sets, showing the constraints on n and r for the MH, LWB, and sudden reionization schemes. When the sudden reionization assumption is relaxed, the mean values of n and r tend to shift to higher values. The shift in n was already noted in the previous paper [6]. The importance of this shift is that in a general reionization scheme the H–Z spectrum is perfectly consistent. Notice, however, that the presence of tensors and/or a running spectral index in the analysis allows for a H–Z spectrum even in the sudden reionization scheme (at a confidence level (c.l.) corresponding to 2σ). Nevertheless, in the case of the MH reionization scenario, without running of the index, the best fit for the scalar spectral index is already higher than one at 68% c.l. In a general reionization scenario the allowed values of r also shift to higher values. When additional data from other CMB probes are added to the WMAP7 data, the constraints on n and r are shifted back toward lower values. In summary, in the MH reionization case ignoring running of the spectral index, using WMAP7 data the H–Z spectrum ($n = 1$) is very close to the best fit value, and inside the 68% c.l. for the case CMB-ALL.

The values for the tensor-to-scalar ratio r and the running of the spectral index n_{run} at 95% c.l. are slightly higher considering a general reionization scenario. However, their 68% c.l. constraints barely change when the

	WMAP7			CMB-ALL			Planck
	Sudden	MH	LWB	Sudden	MH	LWB	Sudden
			no running of scalar spectral index				
n (68% c.l.)	0.987 ± 0.020	1.001 ± 0.027	0.992 ± 0.021	0.974 ± 0.016	0.985 ± 0.020	0.977 ± 0.017	0.960 ± 0.004
n (95% c.l.)	$n \leq 1.031$	$n \leq 1.067$	$n \leq 1.039$	$n \leq 1.007$	$n \leq 1.026$	$n \leq 1.012$	$n \leq 0.968$
r (68% c.l.)	0.142 ± 0.116	0.141 ± 0.119	0.149 ± 0.115	0.095 ± 0.079	0.101 ± 0.085	0.103 ± 0.087	0.053 ± 0.022
r (95% c.l.)	$r \leq 0.373$	$r \leq 0.376$	$r \leq 0.371$	$r \leq 0.251$	$r \leq 0.266$	$r \leq 0.275$	$r \leq 0.093$
			running of scalar spectral index				
n (68% c.l.)	1.067 ± 0.062	1.080 ± 0.065	—	1.094 ± 0.052	1.106 ± 0.054	—	—
n (95% c.l.)	$n \leq 1.192$	$n \leq 1.207$	—	$n \leq 1.197$	$n \leq 1.222$	—	—
r (68% c.l.)	0.191 ± 0.154	0.200 ± 0.158	—	0.181 ± 0.141	0.185 ± 0.140	—	—
r (95% c.l.)	$r \leq 0.497$	$r \leq 0.515$	—	$r \leq 0.451$	$r \leq 0.445$	—	—
$n_{\rm run}$ (68% c.l.)	-0.040 ± 0.029	-0.036 ± 0.031	—	-0.056 ± 0.021	-0.058 ± 0.022	—	—

TABLE I. Constraints for different data sets on n, r, and $r_{\rm run}$ in different reionization scenarios with and without the running of the scalar spectral index n.

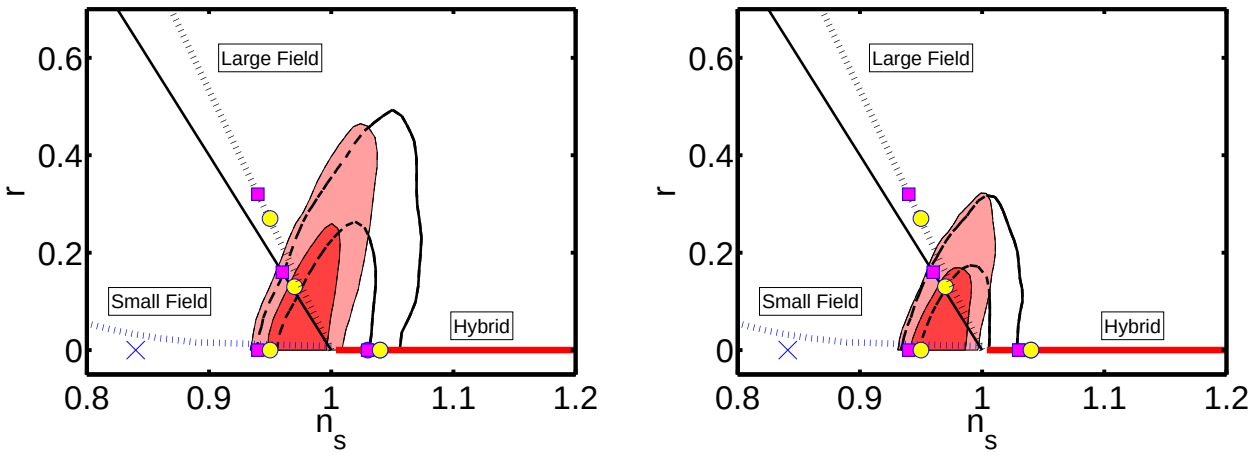

FIG. 1. Two-dimensional contour plots at the 68% and 95% confidence levels without running of the scalar spectral index for the WMAP7 data (left figure) and the CMB-ALL data set (right figure). Shaded contours correspond to the sudden reionization approximation, while open contours model reionization as MH. The dark solid (dashed) lines refer to large-field models with $p = 2$ ($p = 4$). The lighter cross (dashed) curves depict small-field models with $p = 2$ ($p = 4$). The solid horizontal line that basically coincides with the x axis depicts hybrid models with $p = 2$ (the $p = 4$ case basically overlaps the $p = 2$ case). The filled circles (squares) denote the points in the parameter space for which the number of e-folds N is equal to 60 (50).

reionization history is modified, as expected, due to the large uncertainties on r and n_{run}.

The shift induced on allowed values of inflationary parameters n and r by different assumptions for the reionization history is important for the subsequent constraints on inflationary models. To study this, we have reconstructed the relation between n and r in the different classes of models described in the previous section, and we have plotted these relations in the n-r plane, together with the cosmological constraints.

Figure 1 depicts the 68% and 95% c.l. allowed contours by the WMAP7 data and the CMB-ALL data sets

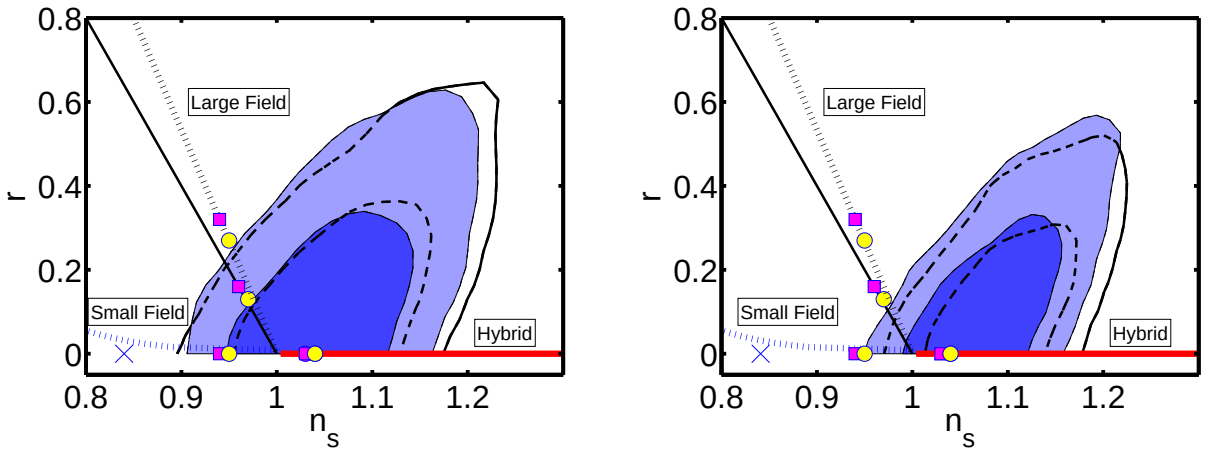

FIG. 2. Two-dimensional contour plots at the 68% and 95% confidence levels with running of the scalar spectral index for the WMAP7 data (left figure) and the CMB-ALL data set (right figure). The key for the figures is the same as in Fig. 1.

without running of the scalar spectral index for different assumptions of the reionization history. The indicated contours denote the allowed regions when tensor modes are included in the analysis, and when the reionization is assumed to be sudden and when using the MH procedure (see the figure caption for details).

Figure 2 is the same as Fig. 1 but now allowing for a running of the scalar spectral index.

Following Ref. [7] we can easily develop the different expressions concerning the n-r parameter space. For instance, for large-field models, with a polynomial potential $V \propto \phi^p$, the relation among these parameters is

$$n = 1 - \frac{r}{8}\left(1 + \frac{2}{p}\right) \ . \tag{24}$$

The dark lines in Figs. 1 and 2 refer to this relation for quadratic ($p = 2$) and quartic ($p = 4$) potentials. It is straightforward to relate r with N (the number of e-foldings before the end of inflation):

$$r = 4p/N \ , \tag{25}$$

which allows us to draw points with $N = 50$ (squares) and $N = 60$ (circles) in Figs. 1 and 2.

Similarly, we can relate n to r, and both of them in terms of N for both small-field and hybrid models. For small-field models, the generic potential we are using is of the form $V(\phi) = \Lambda^4[1 - (\phi/\mu)^p]$. Typically in these models the slow-roll parameter ϵ (and hence, r) is close to zero. The spectral index can be written as

$$n \simeq 1 - \frac{p(p-1)}{4\pi}\frac{m_{Pl}^2}{\mu^p}\left[\frac{\pi\mu^{2p}}{m_{Pl}^2 p^2}\, r\right]^{(p-2)/(2p-2)} \ . \tag{26}$$

It is straightforward to see that for $p = 2$

$$n \simeq 1 - \left(\frac{1}{2\pi}\right)\left(\frac{m_{Pl}}{\mu}\right)^2 \ , \tag{27}$$

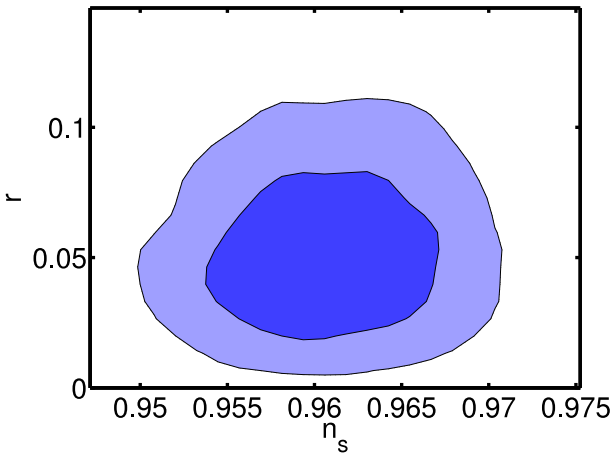

FIG. 3. The 68% and 95% c.l. constraints forecast on the n vs. r plane from Planck mock data for $n = 0.96$ and $r = 0.05$ and sudden reionization (dark contour), and (wrongly) fitted assuming MH reionization (light contour).

while for $p = 4$ we have

$$n \simeq 1 - \frac{3}{\pi}\left(\frac{\pi m_{Pl}^4 r}{16\mu^4}\right)^{1/3} \approx 1 - \frac{3}{N} \ . \tag{28}$$

Figs. 1 and 2 also contain the small-field model case, depicted by cross for $p = 2$ and by the indicated dashed curve for $p = 4$ (assuming $\mu \approx m_{Pl}$).

For hybrid models, the potential chosen is $V(\phi) = \Lambda^4[1 - \alpha(m_{Pl}/\phi)^p]$, based on potentials generated in dynamical SUSY breaking models [16]. As in small-field models, the tensor-to-scalar ratio r is negligible. The expression for n is given by

$$n \approx 1 + 2\frac{(p+1)}{(p+2)(N_{\rm tot} - N)} \ , \tag{29}$$

where $N_{\rm tot}$ is the *total* number of e-foldings (chosen to

be 100 in this example). Notice that Eq. (29) indicates that the power spectrum in these sort of models is blue ($n > 1$). Indeed, in the sudden reionization scenario with negligible running of the spectral index these hybrid models are highly disfavored; in more general reionization schemes such models are allowed by WMAP7 data; see Fig. 1. When more CMB data sets are included in the analysis, hybrid inflation models with a blue tilt are again disfavored at 95% c.l., even in the more general reionization scenarios considered here; see the CMB-ALL part of Fig. 1. When a running scalar spectral index is allowed, hybrid models are perfectly compatible with data, regardless of the assumptions about the reionization processes; see Fig. 2.

The LWB reionization scheme leads to very similar constraints to those of MH parametrization on the $n-r$ plane (albeit slightly closer to the sudden reionization case). Indeed, n is constrained to be red at the 68% c.l. in the CMB-ALL case, but the H–Z model is still consistent with data within two standard deviations.

We also forecast future constraints from the Planck experiment with the specifications of Ref. [17], assuming that $n = 0.96$ and $r = 0.05$ and sudden reionization. If the data is (wrongly) fitted assuming a more general reionization scenario (MH reionization, for instance), the constraints that one would obtain on the $n-r$ plane are shown in Fig. 3. Notice that Planck will be able to tell $n \neq 1$ at a very high confidence level even if the precise details of the reionization processes are unknown. Planck data will also be sensitive to the tensor-to-scalar ratio at the 95% c.l. for $r \geq 0.05$.

VI. MONTE CARLO RECONSTRUCTION OF THE INFLATIONARY POTENTIAL

In this section we describe the technique known as Monte Carlo reconstruction, a stochastic method for inverting observational constraints to obtain an ensemble of inflationary potentials compatible with observations. The method is described in more detail in Refs. [18–20].

The slow roll parameters ϵ and η already have been defined in Sec. II; see Eq. (11). These two parameters are related to the observables n and r by the formulae given in Sec. II, valid to first order in the slow-roll approximation. We find it convenient to use the parameter $\sigma \equiv 2\eta - 4\epsilon$ in place of η; the advantage is that to first order in slow roll, $\sigma \simeq n - 1$.

Taking higher derivatives of H, one can construct an infinite hierarchy of slow-roll parameters [21]:

$$\lambda_{\rm H}^{(\ell)} \equiv \left(\frac{m_{\rm Pl}^2}{4\pi}\right)^{\ell} \frac{(H')^{\ell-1}}{H^{\ell}} \frac{d^{(\ell+1)}H}{d\phi^{(\ell+1)}} \tag{30}$$

The evolution of the slow-roll parameters is described by the following set of equations [18, 22, 23]:

$$\frac{d\epsilon}{dN} = \epsilon(\sigma + 2\epsilon), \tag{31}$$

$$\frac{d\sigma}{dN} = -5\epsilon\sigma - 12\epsilon^2 + 2\lambda_{\rm H}^{(2)}, \tag{32}$$

$$\frac{d\lambda_{\rm H}^{(\ell)}}{dN} = \left[(\ell-1)\frac{\sigma}{2} + (\ell-2)\epsilon\right]\lambda_{\rm H}^{(\ell)} + \lambda_{\rm H}^{(\ell+1)}, \tag{33}$$

Given a solution to these equations, the observable quantities, *i.e.,* the scalar spectral index n, its running n_{run}, and the tensor-to-scalar ratio r, can be evaluated. To second order in slow roll, these are given by [21, 24]:

$$\begin{aligned} r &= 16\epsilon[1 - C(\sigma + 2\epsilon)], \\ n - 1 &= \sigma - (5 - 3C)\epsilon^2 - \frac{1}{4}(3 - 5C)\sigma\epsilon \\ &\quad + \frac{1}{2}(3 - C)\lambda_{\rm H}^{(2)}, \\ n_{run} &= -\left(\frac{1}{1-\epsilon}\right)\frac{dn}{dN}\ , \end{aligned} \tag{34}$$

where $C \equiv 4(\ln 2 + \gamma) - 5 = 0.08145$ and $\gamma \simeq 0.577$ is Euler's constant.

The solution to Eqs. (31-33) also allows one to reconstruct the form of the potential $V(\phi)$ [19, 25–27]. In fact, from the Hamilton–Jacobi equation (see Eq. (11))

$$V(\phi) = \left(\frac{3m_{\rm Pl}^2}{8\pi}\right) H^2(\phi)\left[1 - \frac{1}{3}\epsilon(\phi)\right]. \tag{35}$$

Once $\epsilon(N)$ is known from the solution of Eqs. (31-33), $H(N)$ can be determined from

$$\frac{1}{H}\frac{dH}{dN} = \epsilon. \tag{36}$$

The solution to the above equation allows one then to obtain $V(N)$ up to a normalization constant; this is fixed by the normalization of the Hubble parameter that enters the above equation as a integration constant. We will return on this later.

Finally, in order to obtain $\phi(N)$, we note that Eq. (7) and $dN/dt = -H$ together imply that

$$\frac{d\phi}{dN} = \frac{m_{\rm Pl}^2}{4\pi}\frac{H'}{H} = \frac{m_{\rm Pl}}{2\sqrt{\pi}}\sqrt{\epsilon}, \tag{37}$$

where it should be implicitly understood that there is a sign ambiguity in the last equality since it should have the same sign as $H'(\phi)$. Since we do not know in advance the sign of H', we should consider the two cases separately. However, it is easy to see that they are related by the transformation $\phi \to -\phi$. For this reason, in the following we just consider the case $d\phi/dN < 0$ (i.e, the value of ϕ grows as inflation goes on). Once $\phi(N)$ is obtained from the solution to the above equation, it can be inverted to obtain $N(\phi)$ and finally $V(\phi)$. However, the value of $\phi(N)$ can be known only up to an additive integration

	WMAP7		CMB-ALL	
	Sudden	MH	Sudden	MH
n (99% c.l.)	$0.913 \leq n \leq 1.221$	$0.918 \leq n \leq 1.234$	$0.968 \leq n \leq 1.216$	$0.984 \leq n \leq 1.260$
r (99% c.l.)	$r \leq 0.665$	$r \leq 0.688$	$r \leq 0.551$	$r \leq 0.619$
$n_{\rm run}$ (99% c.l.)	$-0.098 \leq n_{run} \leq +0.037$	$-0.098 \leq n_{run} \leq +0.050$	$-0.099 \leq n_{run} \leq -0.001$	$-0.117 \leq n_{run} \leq -0.001$

TABLE II. Observational limits (at 99% confidence level) used to constrain the inflationary potential for the four cases considered in reconstruction.

constant. We fix the latter so that $\phi = 0$ at the beginning of inflation.

In order to calculate an ensemble of potentials that are compatible with observations, we proceed in the following way:

1. Choose random initial values for the inflationary parameters in the following ranges:

$$\begin{aligned} N &= [40,\, 70] \\ \epsilon &= [0,\, 0.8] \\ \sigma &= [-0.5,\, 0.5] \\ \lambda_{\rm H}^{(2)} &= [-0.05,\, 0.05] \\ \lambda_{\rm H}^{(3)} &= [-0.005,\, 0.005] \\ &\vdots \\ \lambda_{\rm H}^{(6)} &= 0. \end{aligned}$$

   truncated at $M = 6$.

2. Evolve forward in time ($dN < 0$) until either *(a)* inflation ends ($\epsilon > 1$), or *(b)* the evolution reaches a late-time fixed point ($\epsilon = \lambda_{\rm H}^{(\ell)} = 0$, $\sigma = {\rm const}$).

3. In case *(a)*, evolve N e-folds backwards in time from the end of inflation and calculate the observables $n - 1$, r, and the running n_{run} at that time; in case *(b)*, calculate the observables at the time the evolution reaches the fixed point.

4. Repeat the above procedure N_{MC} times.

5. Choose a window of acceptable values for the observables $n - 1$, r, and the running n_{run}, and then extract from the N_{MC} models those that satisfy the observational constraints.

6. Reconstruct the potential for these models, following the procedure described above.

We have implemented the procedure described above with $N_{MC} = 5 \times 10^5$. We consider four sets of observational constraints, corresponding to those obtained in the previous section for the "WMAP7" and "CMB-ALL" datasets in the two cases of sudden and MH reionization scenarios. For convenience, we report four sets of constraints (at the 95% and 99% confidence levels) in Table II. We show a sample of 300 reconstructed potentials in Fig. 4. We have rescaled all the potentials so that $V(\phi = 0) = 1$ and $0 \leq \phi \leq 1$, so that the figure only contains information concerning the shape of the inflationary potential. We see that the WMAP7 data alone do not really constrain the shape of the inflationary potential, even when more general models of reionization are considered. However, the situation changes dramatically when other CMB experiments are included, as it can be seen from the right panels of Fig. 4. Presumably this is due to the fact that when these experiments are included, models with $n_{run} = 0$ are placed outside the observationally allowed region. In this case, the reionization model makes some difference. In the case of sudden reionization the possible shapes of the potential are severely restricted; in particular, it seems that potentials with $V''(\phi) < 0$ are not allowed. When a more general model of reionization is used, however, more shapes are allowed. This is probably an result of the fact that the constraints on the scalar spectral index n are weakened.

Other than the shape of the potential, it is also important to constrain its amplitude. The reconstruction procedure described above does not yield the amplitude of the potential; this has to be fixed from some observational input, like the normalization of the Hubble parameter. We choose to normalize the Hubble parameter through the condition on the density contrast:

$$\frac{\delta\rho}{\rho} \simeq \frac{1}{2\pi}\frac{H}{m_{\rm Pl}}\frac{1}{\sqrt{\epsilon}} \simeq 10^{-5}. \tag{38}$$

Once this is done, we find that in all the four cases illustrated in Table II, $V(\phi) \lesssim 10^{-11}\, m_{\rm Pl}^4$. This correspond to an upper limit to the energy scale of inflation of about $10^{16}\,{\rm GeV}$.

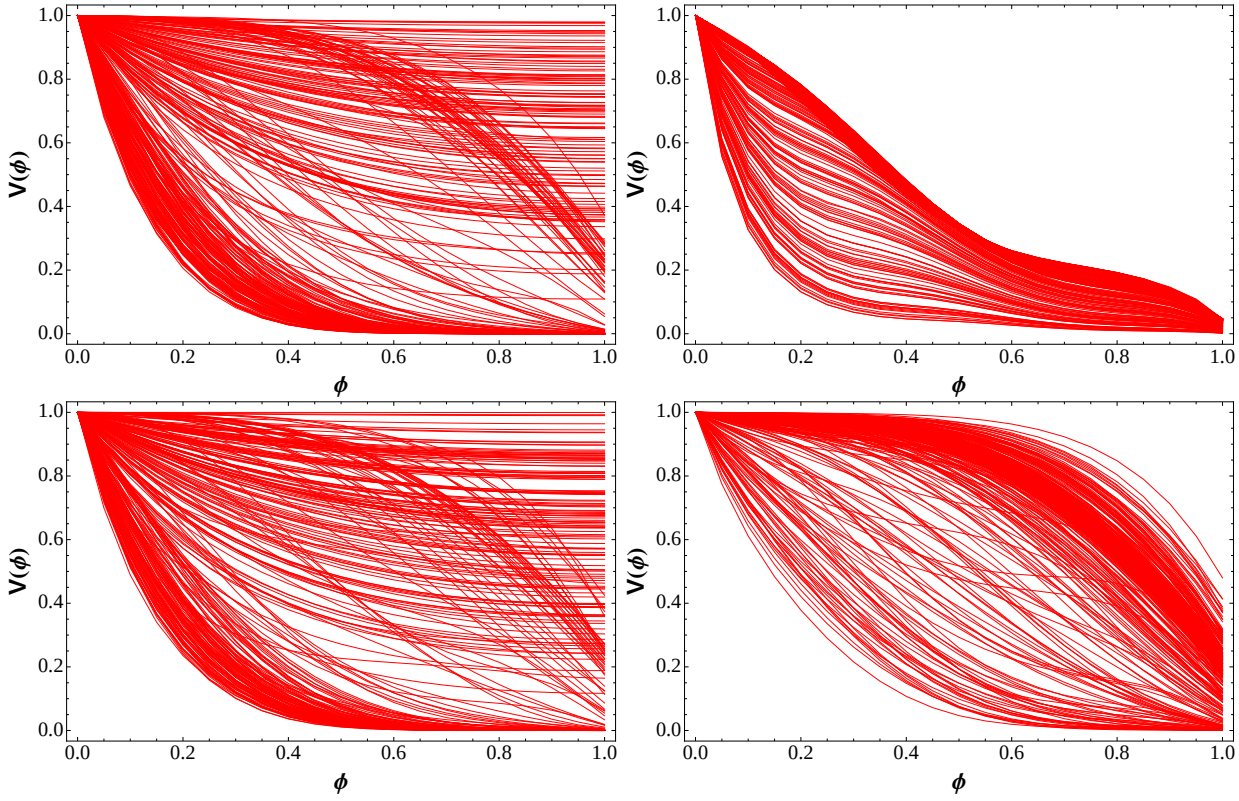

FIG. 4. Sample of three hundred reconstructed potentials for the four sets of observational constraints discussed in the text. The potentials are calculated at the 99% c.l. All the potentials have been rescaled so that $V(\phi = 0) = 1$, and $0 \leq \phi \leq 1$. Upper left panel: WMAP7 with sudden reionization; upper right panel: CMB-ALL with sudden reionization; lower left panel: WMAP7 with MH reionization; lower right panel: CMB-ALL with MH reionization.

VII. CONCLUSIONS

Details of the reionization processes in the late universe are not very well known. In the absence of a precise, full-redshift evolution description of the ionization fraction during the reionization period, a simple parametrization with a single parameter z_r has become the standard reionization scheme in numerical analyses. More general reionization schemes have been shown to allow values of the scalar spectral index consistent with a scale-invariant power spectrum. In this paper we deduce information about tensor modes, and explore how the inflation constraints are modified when the standard reionization assumption is relaxed. The tensor-to-scalar ratio bounds are largely unmodified under more general reionization scenarios. Therefore, present (future) primordial gravitational wave searches are (will be) unaffected by the precise details of reionization processes. In the absence of a running spectral index, hybrid models, ruled out in the standard reionization scheme, are still allowed at the 95% c.l. by WMAP7 data. The constraints on other inflationary models, such as large-field or small-field models, do not change. Future Planck data will be able to measure the scalar spectral index n with unprecedented precision and be sensitive to tensor modes if $r > 0.05$ at the 95% c.l. We also show the impact of different reionization histories on the reconstruction of the inflaton potential. The variety of the reconstructed shapes is larger in extended reionization scenarios than compared to the standard one. Namely, models with $V''(\phi) < 0$ are allowed in general reionization scenarios. However, the constraints on the amplitude of the potential remain unchanged: we find an upper bound for the latter of about 10^{16} GeV, independent of the reionization process details.

ACKNOWLEDGMENTS

We would like to thank William Kinney for useful discussion. O. M. work is supported by the MICINN (Spain) Ramón y Cajal contract, AYA2008-03531 and CSD2007-00060. M. P. is supported by a MEC-FPU Spanish grant.

[1] E. R. Harrison, Phys. Rev. D **1**, 2726 (1970); Y. B. Zel'dovich, Mon. Not. Roy. Astron. Soc. **160**, (1972); P. J. E. Peebles and J. T. Yu Astrophys. J. **162**, 815 (1970).

[2] A. Vallinotto, E. J. Copeland, E. W. Kolb, A. R. Liddle and D. A. Steer, Phys. Rev. D **69**, 103519 (2004); A. A. Starobinsky, JETP Lett. **82**, 169 (2005).

[3] E. Komatsu *et al.*, arXiv:1001.4538 [astro-ph.CO]; D. Larson *et al.*, arXiv:1001.4635 [astro-ph.CO].

[4] M. Zaldarriaga *et al.*, arXiv:0811.3918 [astro-ph].

[5] M. J. Mortonson and W. Hu, Astrophys. J. **686**, L53 (2008) [arXiv:0804.2631 [astro-ph]].

[6] S. Pandolfi *et al.*, Phys. Rev. D **81**, 123509 (2010) [arXiv:1003.4763 [astro-ph.CO]].

[7] W. H. Kinney, E. W. Kolb, A. Melchiorri and A. Riotto, Phys. Rev. D **74**, 023502 (2006) [arXiv:astro-ph/0605338]; W. H. Kinney, E. W. Kolb, A. Melchiorri and A. Riotto, Phys. Rev. D **78**, 087302 (2008) [arXiv:0805.2966 [astro-ph]].

[8] S. Dodelson, W. H. Kinney and E. W. Kolb, Phys. Rev. D **56**, 3207 (1997) [arXiv:astro-ph/9702166].

[9] A. Lewis, J. Weller and R. Battye, Mon. Not. Roy. Astron. Soc. **373** (2006) 561 [arXiv:astro-ph/0606552].

[10] A. Lewis, A. Challinor and A. Lasenby, Astrophys. J. **538**, 473 (2000) [arXiv:astro-ph/9911177].

[11] A. Lewis and S. Bridle, Phys. Rev. D **66**, 103511 (2002) [arXiv:astro-ph/0205436].

[12] W. C. Jones *et al.*, Astrophys. J. **647**, 823 (2006); F. Piacentini *et al.*, Astrophys. J. **647**, 813 (2006), Astrophys. J. **647**, 833 (2006).

[13] M. L. Brown *et al.* [QUaD collaboration], Astrophys. J. **705**, 978 (2009) [arXiv:0906.1003 [astro-ph.CO]].

[14] C. L. Reichardt *et al.*, Astrophys. J. **694**, 1200 (2009) [arXiv:0801.1491 [astro-ph]].

[15] H. C. Chiang *et al.*, Astrophys. J. **711**, 1123 (2010) [arXiv:0906.1181 [astro-ph.CO]].

[16] D. H. Lyth and A. Riotto, Phys. Rept. **314**, 1 (1999). [arXiv:hep-ph/9807278].

[17] [Planck Collaboration], [arXiv:astro-ph/0604069].

[18] W. H. Kinney, Phys. Rev. D **66**, 083508 (2002) [arXiv:astro-ph/0206032].

[19] R. Easther and W. H. Kinney, Phys. Rev. D **67**, 043511 (2003) [arXiv:astro-ph/0210345].

[20] W. H. Kinney, E. W. Kolb, A. Melchiorri and A. Riotto, Phys. Rev. D **69**, 103516 (2004) [arXiv:hep-ph/0305130].

[21] A. R. Liddle, P. Parsons and J. D. Barrow, Phys. Rev. D **50**, 7222 (1994) [arXiv:astro-ph/9408015].

[22] M. B. Hoffman and M. S. Turner, Phys. Rev. D **64**, 023506 (2001) [arXiv:astro-ph/0006321].

[23] D. J. Schwarz, C. A. Terrero-Escalante and A. A. Garcia, Phys. Lett. B **517**, 243 (2001) [arXiv:astro-ph/0106020].

[24] E. D. Stewart and D. H. Lyth, Phys. Lett. B **302**, 171 (1993) [arXiv:gr-qc/9302019].

[25] H. M. Hodges and G. R. Blumenthal, Phys. Rev. D **42**, 3329 (1990).

[26] E. J. Copeland, E. W. Kolb, A. R. Liddle and J. E. Lidsey, Phys. Rev. Lett. **71**, 219 (1993) [arXiv:hep-ph/9304228].

[27] E. Ayon-Beato, A. Garcia, R. Mansilla and C. A. Terrero-Escalante, Phys. Rev. D **62**, 103513 (2000) [arXiv:astro-ph/0007477].